MRI-guided percutaneous cryoablation of the prostate in an animal model: In vivo imaging of cryo-induced tissue necrosis with immediate histolopathological correlation

M.A.A.J. van den Bosch[1], **S. Josan**[2], **D.M. Bouley**[3], **J. Chen**[2], **H. Gill**[4], **V. Rieke**[2], **K. Butts-Pauly**[2], and **B.L. Daniel**[1]

[1)]Department of Radiology, Stanford University, Stanford, California

[2)]Lucas MRS imaging Center, Stanford University, Stanford, California

[3)]Department of Pathology, Stanford University, Stanford, California

[4)]Department of Urology, Stanford University, Stanford, California

Abstract

Purpose: to evaluate the feasibility of Magnetic Resonance Imaging (MRI)-guided percutaneous cryoablation of normal canine prostates and to identify MR imaging features that accurately predict the area of tissue damage at microscopic level.

Methods: Six adult male mixed breed dogs were anesthetized, intubated, and placed in the 0.5T Signa open MRI system. A receive only endorectal coil was placed in the rectum. The prostate's exact location and depth, in relation to skin, was determined on T1-weighted fast spin-echo imaging (FSE) MRI. 17G titanium cryoprobes and Luxtron fiberoptic temperature sensors were stepwise inserted percutaneously into the prostate under MRI guidance. After confirming the correct placement of the cryoprobes and temperature sensors, three different freezing protocols were used to ablate prostate tissue: A) single probe ablation, final temperature between −10°C and −40°C, one freeze/thaw cycle; B) single probe ablation, final temperature below −40°C, two freeze/thaw cycles; C) multiple 4 probe ablation, final temperature between 0°C and −10°C, one freeze/thaw cycle. The size of the ice-ball during cryoablation was monitored with T1-FSE imaging. Directly post-procedural the area of cryo-induced tissue necrosis was assessed with contrast-enhanced weighted MRI and compared to histopathology.

Results: A total of 12 cryolesions (mean size 1.2cm) were bilaterally created in 6 normal canine prostates. Ice-ball formation was oval and imaged signal-free on T1-FSE sequences in all cases. Direct post-procedural contrast-enhanced MRI typically showed a low signal intensity, non-enhancing area, centrally located within the frozen area, surrounded by a bright enhancing rim, in

Correspondence: M.A.A.J. van den Bosch, MD, PhD, Radiological Sciences Laboratory, Lucas MRS Imaging Center, 1201 Welch Road, Stanford, CA 94305-5488, T 650 498 7550, F 650 726 7925, maaj.vandenbosch@gmail.com.

all cases (n=12). On histopathology two distinct zones were identified within the 12 cryolesions by microscopy. Centrally, a necrotic zone with complete cellular destruction and hemorrhage was found (cryo-induced tissue necrosis). Between this necrotic zone and normal glandular tissue, a second zone was seen consisting of fragmented and intact glands, interstitial edema and rare acute inflammatory cells (transitional zone). Overall, the mean area of non-enhancement on contrast-enhanced weighted MR images relative to cryo-induced tissue necrosis on pathology was 0.91. This correlation was consistent within all 6 dogs, i.e. Pearson's correlation coefficient of 0.97.

Conclusion: MRI-guided cryoablation of the prostate is technically feasible. The non-enhancing area on post-ablation contrast-enhanced weighted MRI accurately predicts the area of cryo-induced tissue necrosis on pathology.

Introduction

Cryoablation, i.e. tissue necrosis caused by freezing, is increasingly used for minimally invasive tumor cell destruction (1). Recent advances in non-invasive imaging techniques, including ultrasound (US) and magnetic resonance imaging (MRI), have fueled the interest in image-guided cryoablation for local control of prostate cancer (2–4). The main goal of imaging during the cryoablation procedure is to accurately monitor and control of the extent of the frozen region, i.e. the ice-ball (5).

Cryoablation for treatment of localized prostate cancer is currently carried out under transrectal ultrasound guidance (4). However, ultrasound has some limitations with regard to monitoring the freezing procedure. The critical angle shadowing effect causes the ice-ball to cast a shadow that is larger than the ice-ball itself. As a consequence, the majority of the frozen tissue remains invisible and cell destruction at the rim of the shadow may not be uniformly complete.

Contrary to US, MRI is a more promising cryoablation guidance modality for several reasons. First, experimental studies have proven the capability of MRI for imaging the extent of frozen tissue with high accuracy and excellent contrast between normal and frozen tissue due to the signal void of frozen water on all conventional MRI sequences (6,7). Second, MRI depicts the ice-ball boundaries well in 3 dimensions. Third, MRI potentially allows non-invasive quantitative temperature mapping within the ice-ball and its surrounding tissue, using ultrashort-TE MRI and proton resonance frequency (PRF) shift thermometry, respectively (8). Fourth, contrast-enhanced MRI potentially has the ability to visualize the acute necrotic zone due to lack of perfusion (9).

It has been demonstrated that cell damage is related to the particular thermal parameters experienced during freezing, with cellular death ranging from 0% at the ice-ball boundary to 100% at the center of the ice-ball (10,11). Accurate imaging of the ice-ball with contrast-enhanced MRI is clinically of value, because it could be used to evaluate if repeated or extended treatment is necessary. This experimental study was designed to evaluate the feasibility of MRI-guided percutaneous cryoablation of normal canine prostates and to identify MR imaging features that accurately predict the area of cryo-induced tissue necrosis at histopathologic level.

Methods

All animal experiments were approved by Stanford University's Institutional Animal Care and Use Committee. Six adult male mixed breed dogs were anesthetized, intubated, and placed supine in the 0.5T Signa open MRI system (General Electric Medical Systems, Milwaukee, WI). A receive only endorectal coil was placed in the rectum. 17-gauge MRI compatible cryoablation probes (Galil Medical, PA, USA) and Luxtron (Luxtron Corporation, Santa Clara, CA) and 22G fiberoptic temperature sensors were inserted through the anterior abdominal wall into the normal canine prostate (Figure 1a–b).

The prostate's exact location and depth, in relation to skin, was determined on T1-weighted fast spin-echo imaging (FSE) [echo train length of four, TR/TE 300/8–14 ms [minimum effective], ±16-kHz receiver bandwidth, 256×128 matrix, 5mm section thickness, 10 cm FOV] (12). Cryoprobes and Luxtron fiberoptic temperature sensors were stepwise inserted percutaneously into the prostate. Each step was controlled by using the T1-FSE images as described above. After confirming the correct placement of the cryoprobes and temperature sensors, three different freezing protocols were used to ablate prostate tissue: A) single probe ablation, final temperature between −10°C and −40°C, one freeze/thaw cycle (indicating one ablation with a single probe); B) single probe ablation, final temperature below −40°C, two freeze/thaw cycles (indicating two ablations per probe); C) multiple 4 probe ablation, separated 5mm apart, final temperature between 0°C and −10°C, one freeze/ thaw cycle (indicating one ablation per probe).

Cryoablation was performed using a MRI-compatible cryotherapy system (CryoHit Galil Medical Ltd, Yokneam, Isreal). The cooling mechanism is based on the Joule-Thomson effect (i.e. the temperature decrease of gas during expansion). At a system of 300 bar, room-temperature argon gas expands within the tip of the cryoprobe and causes a temperature decrease of −150°C to −180°C. After passage to the probe tip, the expanding argon gas cools the high pressure argon gas via an heath exchanger and exhaust at room temperature. Because the supplied and exhausted argon gas is at room temperature, no additional thermal insulation of the probe shaft is required. If the system is then driven by helium gas at a pressure of 300 bar, the Joule-Thomson effect is inverted, and the probe tip heats up to 38°C, which allows an active thawing and controlled removal of the probe. The operator unit is installed outside the MRI suite beside the main operator console of the magnet. It is connected to two high-pressure argon- and helium- containing cylinders outside the MRI suite. The operator unit is connected to a separate panel inside the MRI suite next to the scanner by two pressure lines. Before intervention, the sterilized cryoprobes were plugged into the panel inside the MRI suite. In this way, the freezing and thawing process can be started from either outside or inside the MRI suite via remote control.

During freezing the ice formation was continuously imaged with the T1-weighted Fast Spin Echo (FSE) sequence in both axial and coronal planes, and directly post-procedural with contrast-enhanced SPGR (SPoiled Gradient Recalled) T1-weighted images after administration of gadolinium (Magnevis Berlex Laboratories, Montville, NJ) (0.3 mmol/kg). After successful ablation and when no ice was visible on MR images, probes and sensors were removed, and pressure was applied to puncture sites for 5 mintues. Immediately

following the procedure all dogs were sacrificed. Canine prostates were excised, sliced and stained with 1% triphenyl tetrazolium chloride (TTC) solution for 20 minutes at 37°C. The sections were then photographed, transferred 10% buffered neutral formalin, processed for routine paraffin embedding, and stained with hematoxylin and eosin (H&E) staining. The sections were digitally scanned by Trestle corporation at .32 micron/pixel resolution and lesion areas were annotated and measured. MR images were analyzed and manually segmented and reformatted using ImageJ software for windows, after correction for prostate shrinkage following excision, MRI findings were correlated to histopathology.

Comparison of continuous variables was performed with student t-test. For comparison of dichotomous variables the Chi-square test was used. P <0.05 was considered to indicate statistical significance. All statistical analyses were performed with SPSS version 10.0.

Results

The cryoablations were technically successful in all six dogs. A total of 12 cryolesions, with a maximum diameter of 1.2cm (mean) were bilaterally created in 6 normal canine prostates. The ice formation was oval and imaged signal-free on the T1-weighted FSE sequences (Figure 2a and 2b) in all cases (n=12). The interface between the frozen and unfrozen prostate tissue was sharply delineated and allowed precise control of ice-ball formation. Mean maximum ice-ball area was 375 mm^2 for freezing protocol A (single probe ablation, final temperature between −10°C and −40°C, one freeze/thaw cycle), 316 mm^2 for freezing protocol B (single probe ablation, final temperature below −40°C, two freeze/thaw cycles), and 200mm^2 for freezing protocol C (multiple probe ablation, final temperature between 0°C and −10°C, one freeze/thaw cycle), see table 1. Mean treatment time differed according to protocol used, with a mean cryoabaltion time in 12 cases of 20 minutes.

After autopsy and H&E staining of the prostate, two distinct zones were identified within the 12 cryolesions by microscopy (Figure 2d). Centrally, a necrotic zone with complete cellular destruction and hemorrhage was found (cryo-induced tissue necrosis). Between this necrotic zone and normal glandular tissue, a second zone was seen consisting of fragmented and intact glands, interstitial edema and rare acute inflammatory cells (transitional zone).

Ice-formation as reflected by low signal intensity of the T1 FSE images did not predict the tissue damage, i.e. area of cryo-induced tissue necrosis created. For all lesions combined the mean ice-ball diameter was 302 mm^2 compared to 187 mm^2 of cryonecrosis evaluated histologically (table 1).

Direct post-procedural contrast-enhanced MRI (SPGR-sequences) typically showed a low signal intensity, non-enhancing area, centrally located within the frozen area, surrounded by a bright enhancing rim (Figure 2c). The mean maximum area of non-enhancement on contrast-enhanced weighted MRI was 191 mm^2 for freezing protocol A, 191 mm^2 for freezing protocol B, and 95 mm^2 for freezing protocol C. The mean area of non-enhancement as measured on contrast-enhanced MRI relative to mean area of microscopic cryo-induced tissue necrosis was 0.94 (573 mm^2/614 mm^2) for protocol A, 0.91 (1144 mm^2/1264 mm^2) for protocol B, and 0.76 (284 mm^2/371 mm^2) for protocol C. Overall, the

mean area of non-enhancement relative to cryo-induced tissue necrosis was 0.91 (Table 1) indicating that non-enhancement during contrast-enhanced imaging accurately predicts the findings at cellular level. The accuracy was consistent within all six dogs, reflected by a Pearsons correlation coefficient of 0.97 (Figure 3).

Additionally, the low signal intensity area together with the surrounding enhancing rim on contrast-enhanced MRI did exceed the area of the area of ice formation on T1-FSE imaging and necrosis on pathology. Compared to the overall mean area of ice-formation, 302 mm^2, the mean area of low signal intensity plus surrounding contrast-enhanced rim was 328 mm^2, implying that the contrast-enhanced rim reflects damage outside the ice-ball that extends into the surrounding healthy prostate tissue.

Discussion

Prostate carcinoma is the most prevalent malignancy affecting men in the Western world and kills more than 30,000 men a year in the United States (12,13). As a result of prostate-specific antigen (PSA) screening, many men are diagnosed with limited stage disease that is confined to the prostate gland and suitable for local therapy (14,15). Current treatment options for prostate cancer confined to the gland are whole-gland destruction through excision (radical surgery), irradiation (external-beam radiotherapy, brachytherapy), whole-gland ablation (cryoablation) or watchful waiting (16). Considering the current ongoing debate over the best treatment for localized prostate cancer, it would seem that a treatment modality that is less invasive than the traditional therapies might be desirable. Focal cryoablation of the prostate is such a modality that is currently being investigated.

Cryoablation is a technique that uses freezing to achieve in situ tissue necrosis. It is assumed that tissue damage during cryoablation is based on a three-step mechanism. First, ice forms in the extracellular fluid, whereas the intracellular fluid remains unfrozen and supercooled. As the ice forms, the osmolarity of the extracellular fluid increases. Water flows out of the cell to equilibrate this osmolarity, in turn increasing the osmolarity of the intracellular fluid and causing chemical damage to the cell. The degree of chemical damage can be related to the amount of time the cell is exposed to this damaging condition (lethal cell dehydration). Eventually, as the cooling rates increase, the intracellular supercooling results in intracellular ice. This is the second component of damage because intracellular ice results in immediate cell death. Third, freezing results in thrombosis of small blood vessels surrounding the ablation zone with secondary loss of tissue nutrition (17).

Although cryoablation under transrectal ultrasound guidance for whole-gland treatment was first already reported in 1993 (3), only recently has the first study assessing the efficacy of transrectal US-guided focal cryoablation for treatment of localized prostate cancer in nine patients been reported (14). At a mean follow-up of 36 months, 7/9 patients (78%) were potent and had achieved a stable PSA, of these 6/7 patients (86%) underwent post-treatment biopsy that revealed no evidence of residual disease. In a more recent study of Bahn et al. 31 patients with unilateral focal prostate cancer, identified by color Doppler ultrasound, underwent focal transrectal US-guided cryoablation for treatment of the disease (15). At a mean follow-up of 70 months, a stable PSA level was maintained by 26/28 (93%) of patients

and a 96% (24/25) negative biopsy rate was observed. The one biopsy positive patient was subsequently treated with whole-gland cryoablation and remains disease free.

However, all studies assessing transrectal US guidance for either whole-gland or focal cryoabaltion, concluded that US is inadequate for monitoring the freezing process because of the shadow cast by the ice-ball which is significantly greater in size than the ice-ball itself (14,15,18–20). As a consequence, the majority of the frozen tissue remains invisible and cell destruction at the rim of the shadow may not be uniformly complete. As a cryoablation guidance modality, MRI may be more suitable for several reasons. First, MRI provides excellent contrast between normal and frozen tissue on all conventional sequences due to the signal void caused by ice. Second, MRI depicts the ice-ball boundaries well in 3 dimensions (6,7,21). Although MRI-guided cryoablation of the prostate has not been reported before, a few previous studies assessed the value of MRI for imaging prostate tissue necrosis after transrectal US-guided cryoablation. Vellet et al. reported in 8 patients that the region of nonenhancement on post-procedural contrast-enhanced weighted MRI corresponded histologically to coagulative necrosis caused by the cryoablation (2). Kalbhen et al. reported on MRI findings after transrectal US-guided cryoablation for treatment of prostate cancer in 27 patients (9). MR images in 14/27 patients (52%) showed areas of necrosis within the prostate. Shrinkage of the prostate volume by 52% was seen in these patients 8 weeks after cryoablation. Since, prostates were not excised in this study, no differentiation between acute cryo-induced tissue necrosis and transition zone within each cryolesion was made. Contrary to these results, more recently, Donelly et al. assessed if non-enhancing tissue on contrast-enhanced MRI obtained 3 weeks after cryoablation of the prostate could predict nonviable cryoablated tissue at 6-month biopsy (22). In their study 54 patients underwent transrectal US-guided cryoablation of prostate adenocarcinoma, with 49 patients that underwent biopsy at 6 months follow-up. Results showed that findings of postoperative contrast-enhanced MRI were not predictive of 6 months biopsy results, i.e. a signal void on contrast-enhanced MRI did not indicate an avascular gland, nor did it confirm cell death. Although these results were in contrast with their own findings reported in 1997 (2), they provided several possibilities that could explain their results. First, small islands of possibly hypoxic residual tissue could exist that are beyond the resolution of MRI or that do not demonstrate detectable enhancement. Second, incompletely destroyed cancer cells at the margin of the frozen tissue may grow back into the necrotic zone. Third, freezing sensitivity is known to be cell specific and related to rate of freezing, absolute temperature reached and the warming rate. With an increased ablation area obtained in cases that were deeply cooled, i.e. below –40°C, or underwent multiple (>1) freeze-thaw cycles. However, the MR images were acquired with a 0.5T imager and a body coil. It is known that using an endorectal coil, as we did in our study, is preferred for prostate imaging because of higher resolution and a signal-to-noise ratio than body coils.

The results of this study demonstrate that MRI-guided percutenous cryoablation of the prostate is technically feasible, and MRI allows accurate monitoring of the freezing process in 3D. As frozen tissue appears nearly signal free on all MR sequences, a precise delineation of the interface between frozen and unfrozen tissue is possible. In the present study T1-weighted FSE sequences have been successfully applied for monitoring of the cryoablation procedure, allowing clear visualization of the ice-ball size, reflected as a low signal intensity

zone on the T1-weighted images. However, we also found that the ice-ball size was larger than the size of the actual area of acute cryo-induced tissue necrosis.

The zone of necrosis is more accurately visualized with contrast-enhanced MRI. The mean area of necrosis relative to the mean avascular zone of the ice-ball on contrast-enhanced MRI for all cases was 91%. These findings also indicate that a rim of prostate tissue cells is frozen but are not damaged enough by low temperatures to induce complete cell death (transition zone). This zone typically consists of residual prostate epithelial cells, basal cells, or glands with intact basement membranes potentially allowing prostate tissue to regenerate after cryoablation. Based on our preliminary study results it can be concluded that contrast-enhanced MRI of the immediate cryolesion is thus a more useful predictor of the region of tissue damage induced by low temperatures than conventional MR sequences that rely on the signal void from frozen tissue.

In this feasibility study we used cryablation to induc e necrosis in healthy canine prostate tissue. Although in this model, contrast-enhanced MRI clearly predicted the area of necrosis due to freezing, the results should be interpreted with caution when extrapolation to tumor models is made, since it is known that tumor cells are more resistant to low temperatures than normal parenchymal tissue and may survive in necrotic regions of ablated tissue. This would be an interesting area for future studies on MRI-guided prostate cryoablation. If it can be proven that contrast-enhanced MRI can also be reliably used to predict tissue necrosis after cryoablation of prostate cancer in an animal model, translation of this novel technology towards treatment of patients can become reality.

In conclusion, the volume of the ice-ball produced during cryoablation of normal canine prostates as imaged with conventional MRI sequences does not correspond to the volume of tissue necrosis induced by the low temperatures. Contrast-enhanced MRI is a more reliable method for prediction of prostate tissue damage following cryoablation, with an accuracy of 91%.

Acknowledgments

References

1. Onik G Image-guided prostate cryosurgery: state of the art. Cancer Control 2001;8:522–531. [PubMed: 11807422]

2. Vellet AD, Saliken J, Donnelly B, et al. Prostate cryosurgery: Use of MR imaging in evaluation of success and technical modifications. Radiology 1997;203:653–659. [PubMed: 9169684]

3. Onik GM, Cohen JK, Reyes GD, Rubinsky B, Chang Z, Baust J. Transrectal ultrasound-guided percutaneous radical cryosurgical ablation of the prostate. Cancer 1993;72:1291–1299. [PubMed: 7687922]

4. Saliken JC, Donnelly BJ, Brasher P, Ali-Ridha N, Ernst S, Robinson J. Outcome and safety of transrectal US-guided percutenous cryotherapy for localized prostate cancer. J Vasc Interv Radiol 1999;10:199–208. [PubMed: 10082109]

5. Matsumoto R, Oshio K, Jolesz FA. Monitoring of laser and freezing induced ablation in the liver with T1-wieghted MR imaging. J Magn Reson Imaging 1992;2:555–562. [PubMed: 1392248]

6. Tacke J, Adam G, Haage P, Sellhaus B, Gunther RW. MR-guided percutaneous cryotherapy of the liver: in vivo evaluation with histologic correlation in an animal model. J Magn Reson Imaging 2001;13:50–56. [PubMed: 11169803]

7. Tuncali K, Morrison PR, Tatli S, Silverman SG. MRI-guided percutaneous cryoablation of renal tumors: use of external manual displacement of adjacent bowel loops. Eur J Radiol 2006;59:198–202. [PubMed: 16716551]

8. Wansapura JP, Daniel BL, Vigen KK, Butts K. In vivo MR thermometry of frozen tissue using R2* and signal intensity. Acad Radiol 2005;12:1080–1084. [PubMed: 16112510]

9. Kalbhen CL, Hricak H, Shinohara K, et al. Prostate carcinoma: MR imaging findings after cryosurgery. Radiology 1996;198:807–811, [PubMed: 8628875]

10. Bischof J, Christov K, Rubinsky B. A Morphological study of cooling rate response in normal and neoplastic human liver tissue: cryosurgical implications. Cryobiology 1993;30:482–492. [PubMed: 8252916]

11. Tatsutani K, Rubinsky B, Onik G, Dahiya R. Effect of thermal variables on frozen human primary prostatic adenocarcinoma cells. Urology 1996;48:441–447. [PubMed: 8804499]

12. Butts K, Daniel BL, Chen L, et al. Diffusion-weighted MRI after cryosurgery of the canine prostate. J Magn Reson Imaging 2003;17:131–135. [PubMed: 12500282]

13. Cohen JK. Cryosurgery of the prostate: techniques and indications. Rev Urol 2004;6:S20–26.

14. Onik G, Narayan P, Vaughan D, et al. Focal "nerve-sparing" cryosurgery for treatment of primary prostate cancer: A new approach to preserving potency. Urology 2002;60:109.

15. Bahn DK, Silverman P, Lee F, et al. Focal prostate cryoablation: Initial results show cancer control and potency preservation. J Endo Uro 2006;20:688–692.

16. Eggener SE, Scardino PT, Carroll PR, et al. Focal therapy for localized prostate cancer: a critical appraisal of rationale and modalities. J Urol 2007;178:2260–2267. [PubMed: 17936815]

17. Mazur P Cryobiology: the freezing of biological systems. Science 1970;68:939–949.

18. Rukstalis DM, Goldknopf JL, Crowley EM, Garcia FU. Prostate cryoablation: A scientific rationale for future modifications. Urology 2002;60:19 [PubMed: 12206844]

19. Prepelica KL, Okeke Z, Murphy A, Katz AE. Cryosurgical ablation of the prostate: high-risk patient outcomes. Cancer 2005;103:1625–1630. [PubMed: 15747374]

20. Schmidt JD, Doyle J, Larison S. Prostate cryoablation: update 1998. Cancer J Clin 1998;48:239–253.

21. Rubinsky B, Gilbert JC, Onik G, Roos MS, Wong STS, Brennan KM. Monitoring cryosurgery in the brain and in the prostate with proton NMR. Cryobiology 1993;30:191–199. [PubMed: 8319488]

22. Donnelly SE, Donnelly BJ, Saliken JC, Raber EL, Vellet AD. Prostate cancer: gadolinium-enhanced MR imaging at 3 weeks compared with needle biopsy at 6 months after cryoablation. Radiology 2004;232:830–833. [PubMed: 15273337]
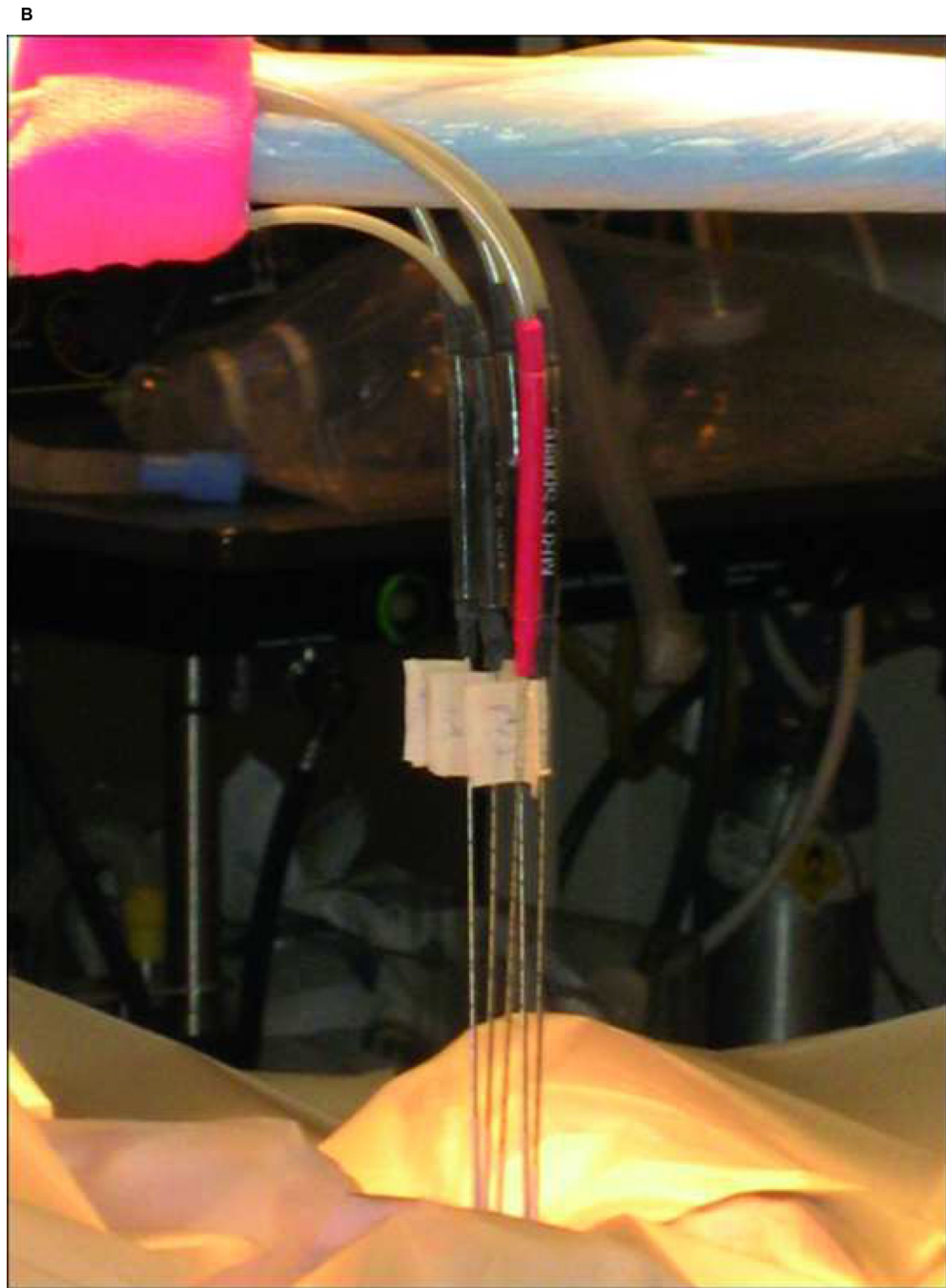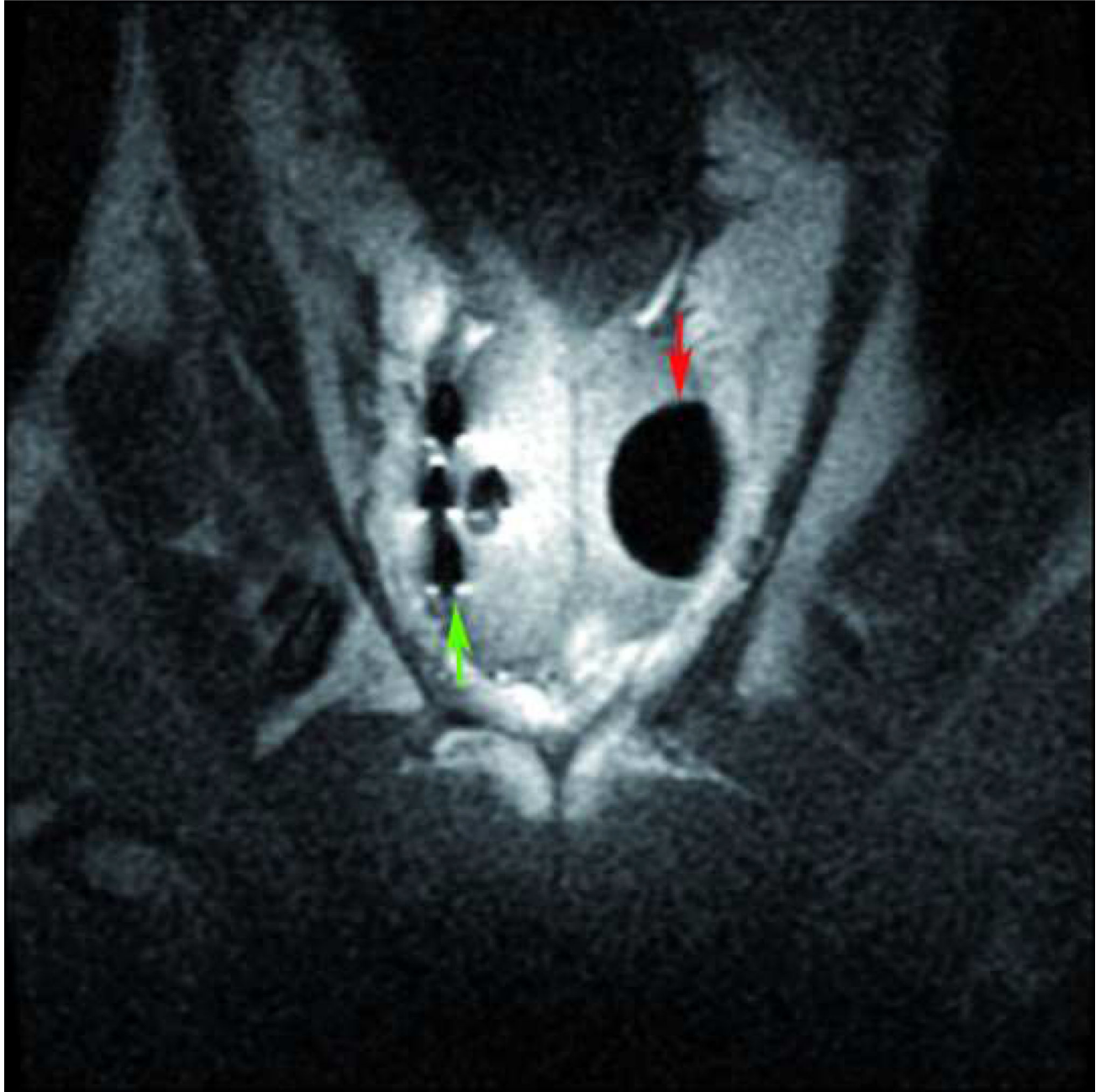
A

B

Fig. 1:
A) The open 0.5T MR imager (Signa-SP, General Electric Medical Systems, Milwaukee, Wisconsin). B) 17-gauge MRI compatible cryoablation probes were percutaneously inserted thorough the anterior abdominal wall.
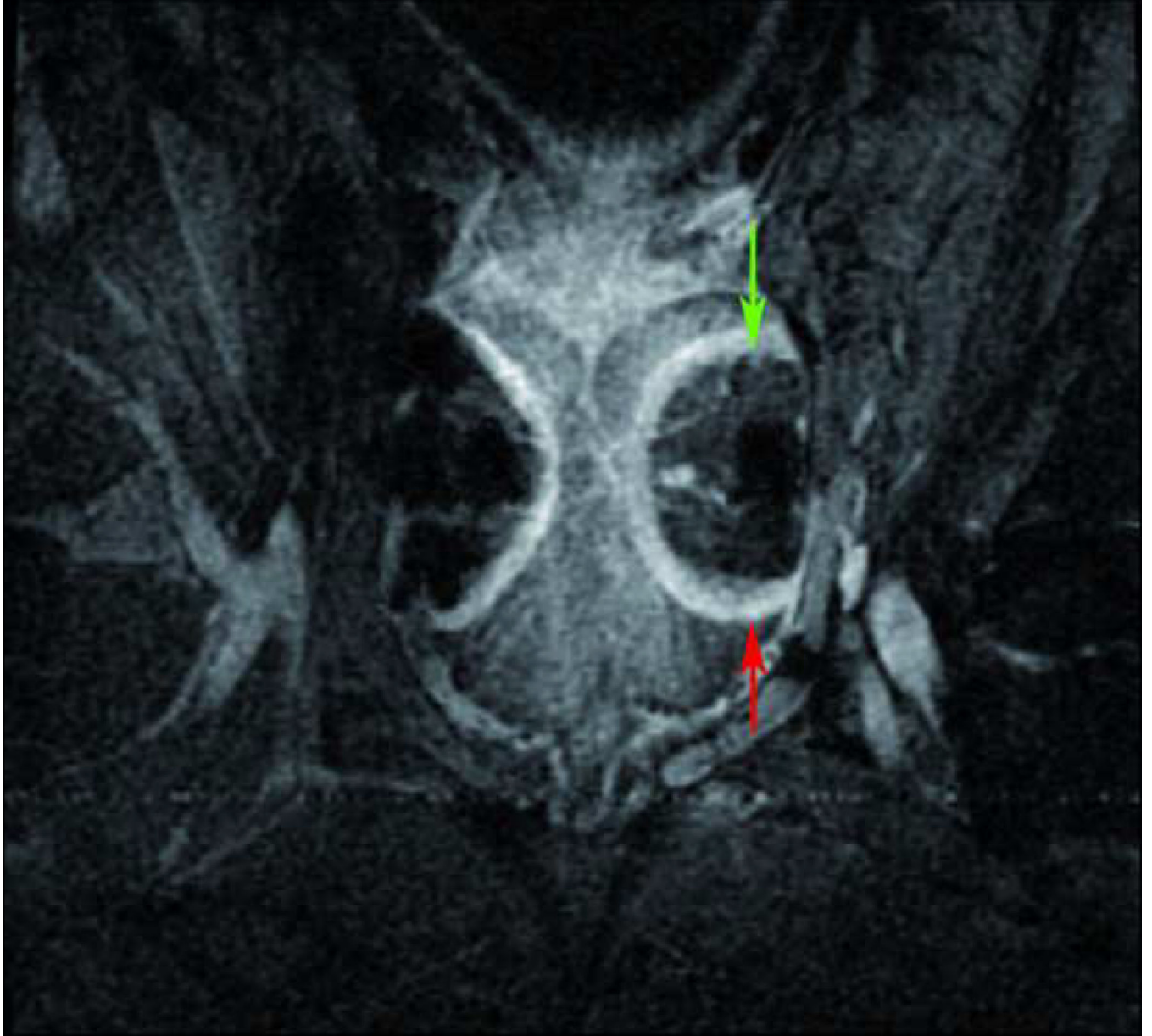
A

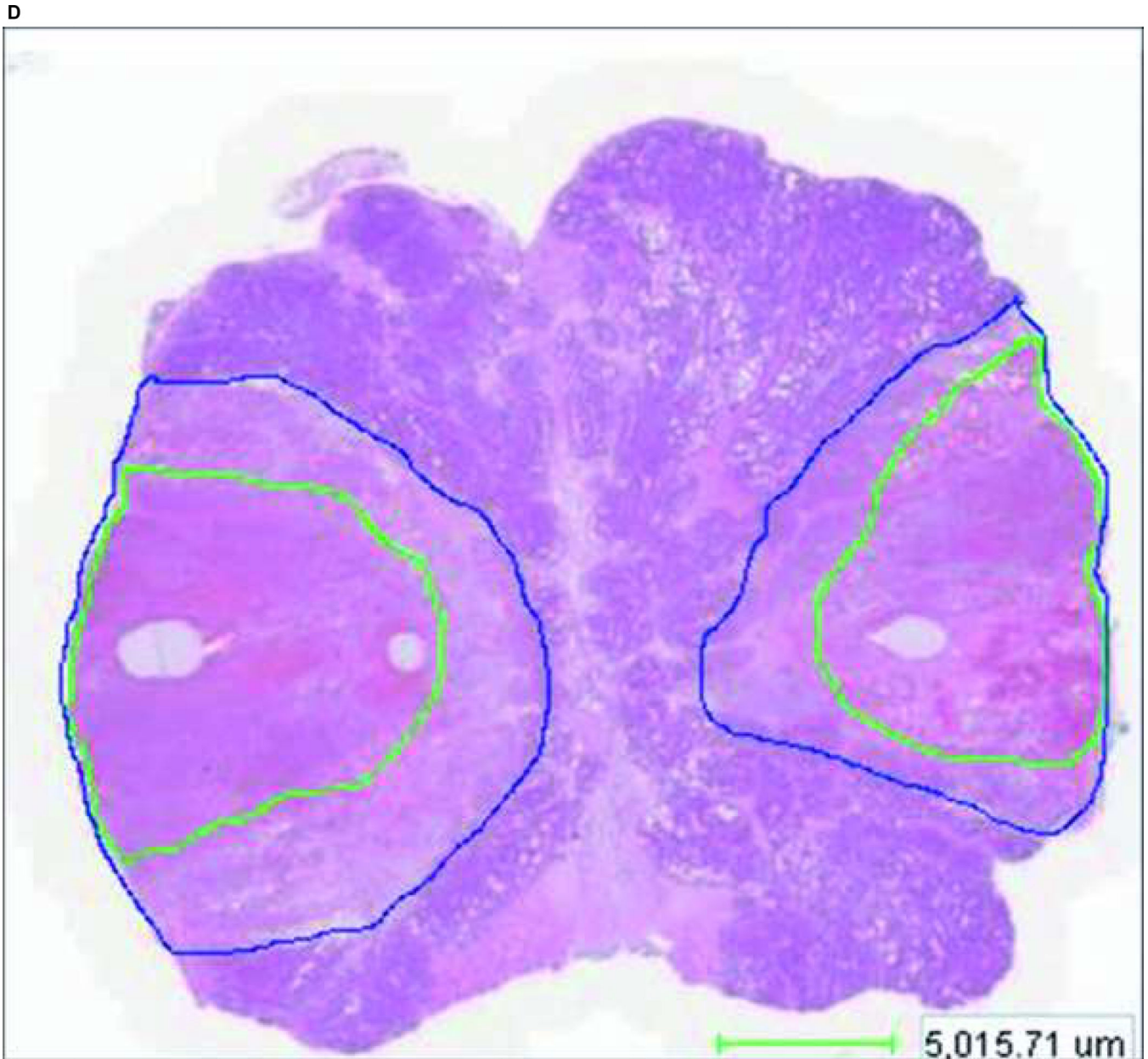**B**

C

D

5,015.71 um

Fig. 2:
Case 4: A) Maximum ice ball size, reflected as low signal intensity zone on T1 FSE MRI (red arrow), created by multiple probe ablation in the right side of the canine prostate. B) Maximum ice ball created by single probe ablation on the left side of the canine prostate (red arrow), and artifacts of multiple probes on the right side (green arrow). C) Avascular zone within the ice ball, reflected as low signal intensity zone (green arrow) surrounding by a high signal intensity rim on contrast-enhanced (SPGR) T1-weighted imaging (red arrow). D) Area of necrosis (green line) on pathology.
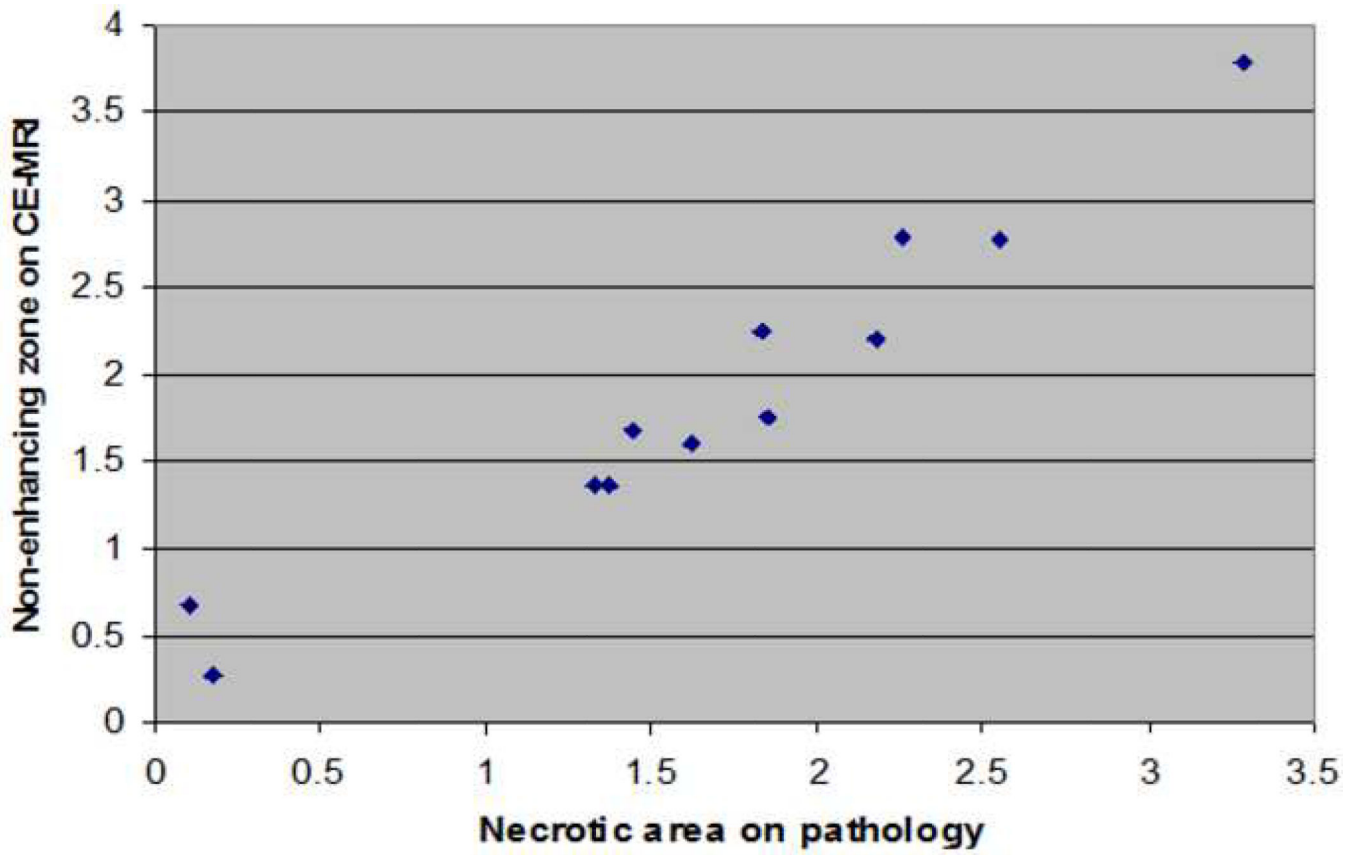
Fig. 3:
Correlation between the area of necrosis on pathology (cm^2) and area of non-enhancement on contrast-enhanced weighted MRI (cm^2)

Table 1.

Ice Formation and Tissue Damage

Case	Freeze Protocol	Side	T1 FSE Low SI area	SPGR Low SI area[*]	SPGR Low SI and high intensity rim area	Pathology: Area of necrosis[*]
1	A	Right	286 mm^2	**162 mm^2**	356 mm^2	**160 mm^2**
	B	Left	358 mm^2	**218 mm^2**	359 mm^2	**220 mm^2**
2	A	Right	334 mm^2	**185 mm^2**	340 mm^2	**176 mm^2**
	B	Left	299 mm^2	**133 mm^2**	321 mm^2	**137 mm^2**
3	A	Right	505 mm^2	**226 mm^2**	393 mm^2	**278 mm^2**
	B	Left	419 mm^2	**183 mm^2**	298 mm^2	**224 mm^2**
4	C	Right	282 mm^2	**255 mm^2**	491 mm^2	**277 mm^2**
	B	Left	341 mm^2	**329 mm^2**	408 mm^2	**379 mm^2**
5	C	Right	136 mm^2	**11 mm^2**	158 mm^2	**67 mm^2**
	B	Left	287 mm^2	**137 mm^2**	241 mm^2	**136 mm^2**
6	C	Right	183 mm^2	**18 mm^2**	259 mm^2	**27 mm^2**
	B	Left	197 mm^2	**144 mm^2**	309 mm^2	**168 mm^2**

[*] Correlation between low signal intensity area on contrast-enhanced weighted imaging (SPGR) and area of necrosis on pathology was R=0.97